PPPL-2414

PPPL-2414

UC20-A,D

PLASMA TRANSPORT IN A COMPACT IGNITION TOKAMAK

By

C.E. Singer, L-P. Ku, and G. Bateman

FEBRUARY 1987

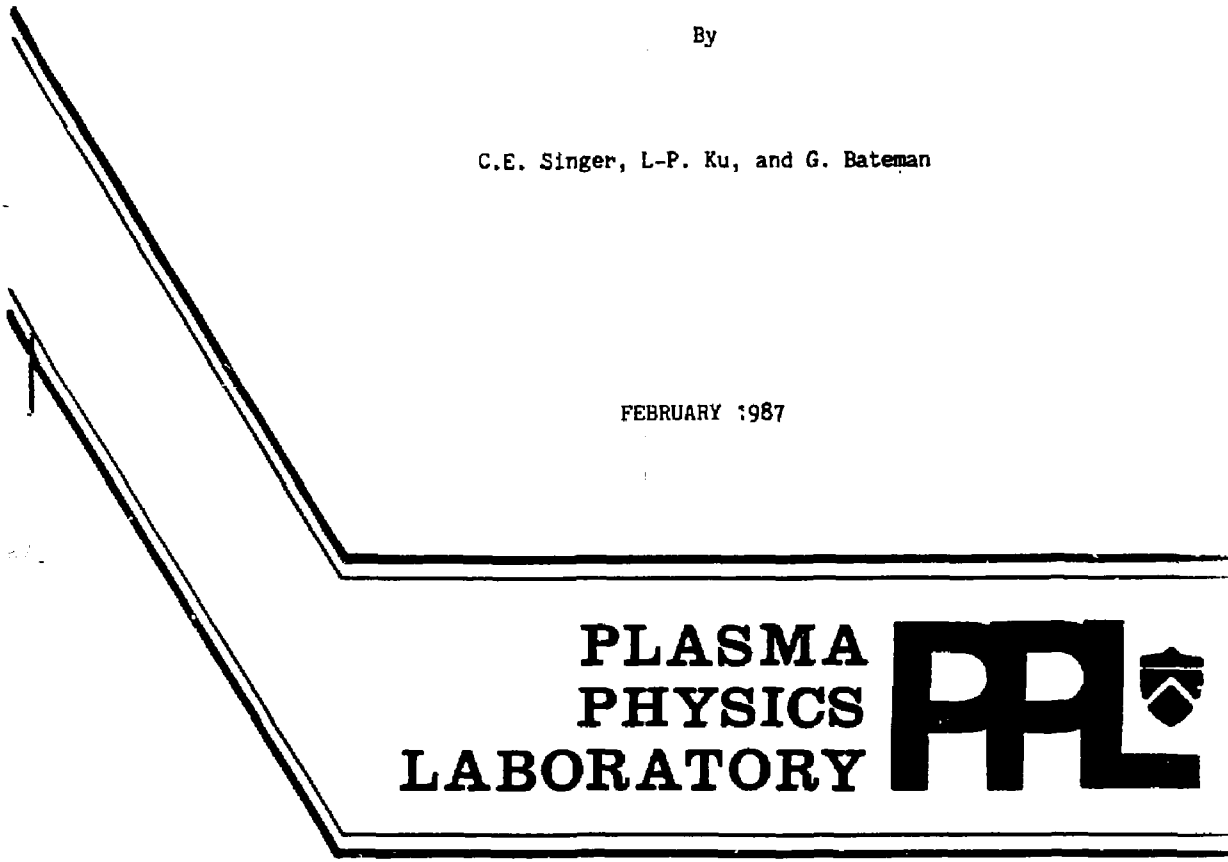

PRINCETON UNIVERSITY
PRINCETON, NEW JERSEY

PREPARED FOR THE U.S. DEPARTMENT OF ENERGY,
UNDER CONTRACT DE-AC02-76-CHO-3073.

Plasma Transport in a Compact Ignition Tokamak

C. E. Singer,
University of Illinois
Urbana, IL 61801

PPPL--2414
DE87 008068

L–P. Ku and Glenn Bateman
Plasma Physics Laboratory, Princeton University
Princeton, NJ 08544

Nominal predicted plasma conditions in a compact ignition tokamak are illustrated by transport simulations using experimentally calibrated plasma transport models. The range of uncertainty in these predictions is explored by using various models which have given almost equally good fits to experimental data. Using a transport model which best fits the data, thermonuclear ignition occurs in a Compact Ignition Tokamak design with major radius 1.32 m, plasma half–width 0.43 m, elongation 2.0, and toroidal field and plasma current ramped in six seconds from 1.7 to 10.4 T and 0.7 to 10 MA, respectively. Ignition is facilitated by 20 MW of heating deposited off the magnetic axis near the ^{3}He minority cyclotron resonance layer. Under these conditions, sawtooth oscillations are small and have little impact on ignition. Tritium inventory is minimized by preconditioning most discharges with deuterium. Tritium is injected, in large frozen pellets, only after minority resonance preheating. Variations of the transport model, impurity influx, heating profile, and pellet ablation rates, have a large effect on ignition and on the maximum beta that can be achieved.

I. INTRODUCTION

The Compact Ignition Tokamak (CIT) is designed to explore the physics of fusion ignition for close to the minimum possible cost. To accomplish this, the engineering design teams have tried to choose nearly the smallest machine size compatible with ignition. The initial design has necessarily been done with relatively simple prescriptions for the limits on global confinement, the ratio of thermal to magnetic pressure, plasma density, etc.[1]

This paper examines the range of expected plasma performance in a compact ignition device. The focus will be on using transport models which are more complete and better calibrated against experiments than those used in the preliminary studies referred to above. The machine parameters examined are given in Table I. These come from a systems code analysis and are representative of designs under consideration for construction.[2] We use two types of transport models: empirical[3] and semiempirical.[4] Each model has radial variation of diffusion coefficients aimed at reproducing experimental plasma profiles. Both models are synoptic, in the sense that they are based on energy confinement scalings from both ohmic and auxiliary heating. Both models have been coded into the same upgraded 1-1/2-D version of the BALDUR transport code.[5,6]

The version of the BALDUR code used here solves the flux-surface-average transport equations[5]

$$\frac{1}{V'}\frac{\partial(V'n_a)}{\partial t}\bigg|_{\psi_{\rm tor}} + \frac{1}{V'}\frac{\partial(V'\langle\Gamma_a\cdot\nabla\rho\rangle)}{\partial\rho} = S_a, \tag{1}$$

$$\frac{3}{2}\frac{1}{(V')^{5/3}}\frac{\partial[(V')^{5/3}n_jT_j]}{\partial t}\bigg|_{\psi_{\rm tor}} + \frac{1}{V'}\frac{\partial[V'\langle(-n_j\chi_j\nabla T_j + c_jT_j\Gamma_j)\cdot\nabla\rho\rangle]}{\partial\rho} = S_j, \tag{2}$$

$$\frac{\partial\psi}{\partial t}\bigg|_{\psi_{\rm tor}} = \frac{\eta RB_T}{\mu_o V'\langle 1/R^2\rangle}\frac{\partial}{\partial\rho}\left[\frac{V'\psi'}{RB_T}\left\langle\frac{|\nabla\rho|^2}{R^2}\right\rangle\right], \tag{3}$$

where V is the volume within a flux surface labelled by ρ. $V' = \partial V/\partial\rho$. $\langle\cdots\rangle$ is the flux surface average operator, ψ is the poloidal flux per unit radian ($\psi_{\rm pol}/2\pi$), and RB_T is the major radius times toroidal field. Here, all time derivatives and all transport fluxes are taken relative to surfaces

with constant toroidal flux, and ρ must be a function of toroidal flux independent of time. Additional convection terms are introduced when these equations are rewritten using any other convenient flux surface label (such as half-width). The following quantities are appropriately averaged over each magnetic surface: the partial and total ion densities n_a and n_i, the ion particle fluxes and sources Γ_a and S_a, the ion and electron thermal diffusivities χ_i and χ_e, the ion and electron temperatures (in joules) T_i and T_e, the ion and electron energy sources S_i and S_e, and the parallel neoclassical resistivity η. The magnetic surfaces are computed using a scalar pressure equilibrium moments code.[7-9]

Throughout this paper, we take

$$\Gamma_a = -D_a \nabla n_a + \Gamma_a^{neo}, \tag{4}$$

$$\chi_i = \alpha_i \chi_e + \chi_i^{CH}, \tag{5}$$

$$c_i = c_e = 3/2, \tag{6}$$

where α_i is normally chosen to be 0.2. Here Γ_a^{neo} includes the Ware pinch for hydrogen isotopes[6] and the remaining neoclassical fluxes for all species from the banana-plateau formulas of Hawryluk et al.[10] Each impurity is treated as a single type of ion, whose charge is given by coronal equilibrium. For the ion thermal diffusivity χ_i^{CH} of Chang and Hinton,[11] we use $\epsilon = r/R$, where R is the midpoint of the flux surface and r is the half-width. Other neoclassical contributions to energy transport are neglected. The convection coefficients $c_i = c_e = 3/2$ are appropriate for at least some types of turbulent transport.[12,13]

Auxiliary heating is concentrated within ± 5 cm of the initial and final ^{3}He cyclotron resonance, located at $r = a/2$ in the reference simulations below (where a is the half-width of the bounding flux surface). The distribution of the auxiliary heating is 75% to the ions and 25% to the electrons.[3] This version of BALDUR assumes concentric circular flux surfaces for the Monte-Carlo computation of neutral transport[14] and first orbit losses and slowing down of fast alpha particles.[15]

In succeeding sections of this paper, we describe the diffusion coefficients used, and we explain to what extent they have been calibrated against experimental data. We then show reference CIT discharge simulations and illustrate the effect of variations in the transport coefficient scaling, impurity concentration, pellet ablation, heating profile, and sawtooth period.

The accuracy of the transport models and stability of the resulting plasma profiles are then discussed. Finally, we discuss implications for CIT design and operation, and the need for further analysis.

II. TRANSPORT MODELS

Here we use transport coefficients based on both ohmic and non-ohmic heating discharges. This is necessary because the global skin time $t_{skin} = \pi a^2 \kappa_a / (10^7 \eta)$ for our CIT parameters,

$$t_{skin} \sim (T_{keV})^{3/2} \tag{7}$$

is comparable to the discharge time, even before auxiliary heating. The temperature profile during ohmic heating could therefore have a persistent influence on the radial profile of the plasma current.

We limit ourselves to two sets of transport coefficients, which we refer to as the "empirical" and the "semiempirical" models, which have previously been tested (directly or indirectly) against a variety of experimental data. The first set is from a purely empirical model based primarily on the global energy confinement scaling described by Kaye and Goldston.[16] The second set of transport coefficients comes from the direct experimental calibration of a semiempirical model based on the work of Pfeiffer and Waltz.[17] The comparison of predictions from these models with experimental data is described in detail elsewhere.[18] The relation of this semiempirical model to theory is discussed below.

A. Empirical Model

1. Transport Coefficients

Houlberg[3] has extensively modelled earlier versions of CIT with an empirical transport model based, in part, on a global energy confinement scaling described by Kaye and Goldston[16]

$$\tau_E^{aux} = 3.82 \times 10^{-11} \frac{I^{1.24} R_o^{1.65} \kappa_a^{0.28} (\overline{n}_e)^{0.26}}{P^{0.58} Q^{0.49} B_o^{0.09}}. \tag{8}$$

where I is the toroidal plasma current, κ_a is the ratio of maximum height to width of the bounding flux surface, B_o is the toroidal magnetic field, R_o is the major radius to the midpoint of the bounding flux surface, $\overline{n}_e$ is the line-average electron density along the midplane, and P is the total heating power (without correction for radiative losses). (All quantities here and below are in SI units except where indicated in the text.) This formula for τ_E^{aux} is scaled with the arithmetic mean ion mass (in amu) and is combined as the inverse square with an approximate ohmic scaling,

$$\tau_E^{OH} = 7 \times 10^{-22} \overline{n}_e R_o a^2 q_{cyl} \tag{9}$$

to give

$$\tau_E = \left[(\tau_E^{OH})^{-2} + \left(\alpha_{LH} \tau_E^{aux} \sqrt{A_i/1.5} \right)^{-2} \right]^{-1/2}. \tag{10}$$

For application in BALDUR, we take[19]

$$q_{cyl} = 2.5 \times 10^6 [1 + \kappa_a^2 (1 + 2\delta_a^2)][a^2 B_o/(R_o I)]$$

and we take A_i to be the arithmetic mean ion mass (in amu), averaged over the plasma volume. For a heuristic, empirical, high confinement mode (H-mode) model, we retain the same boundary flux surface and follow Houlberg by setting $\alpha_{LH} = 2$.

The diffusion coefficients in our implementation of this empirical model are

$$\chi_e = \frac{\kappa_a^2 (\rho^2 + a^2/4)}{(1 + \kappa_a^2) \tau_E}. \tag{11}$$

$$\chi_i = 0.2 \chi_e + \chi_i^{CH}, \tag{12}$$

$$D_a = 0.2 \chi_e. \tag{13}$$

There are some minor differences between our implementation of this model and Houlberg's.[3] We use line-averaged density ($\overline{n}_e$) instead of volume averaged ($\langle n_e \rangle$), and $2\kappa_a^2/(1+\kappa_a^2)$ instead of the local flux surface average geometry factor $1/\langle (\nabla \rho)^2 \rangle$. These should be 10 – 20% effects for the CIT ignition simulations shown here. Houlberg[2] has also included a small anomalous pinch term, which is not included here. The formulas used here reproduce the value of τ_E from Eq. (10) at the maximum achieved $\langle \beta \rangle$ with $\alpha_{LH} = 1$ when used in BALDUR for the CIT simulations shown here.

Houlberg needed a somewhat larger leading coefficient when similarly using the WHIST code to match τ_E in Eq. (10) for an earlier set of CIT parameters.

2. Prescribed Conditions

The time evolutions of the boundary conditions and constraints used in our simulations are shown in Fig. 1. The plasma is initiated at time $t = 0$ with $I = 0.7$ MA plasma current, $B_o = 1.7$ T toroidal field, and $\langle n \rangle = 4.0 \times 10^{19} \mathrm{m}^{-3}$. The vacuum toroidal field rises rapidly at first and then more slowly in order to approximate a linear rise in the toroidal magnetic energy, consistent with the power supplies available. The linear rise, flat top, and fall of the toroidal plasma current are consistent with the poloidal field coil systems in the design. A maximum volume average density of 6×10^{20} m^{-3} was chosen for simulations with the empirical model on the basis of Houlberg's work.[3] During start-up, the volume average density was constrained to be

$$\langle n_e \rangle \leq 0.5 \frac{10^{14} I}{\pi a^2}. \tag{14}$$

which leaves a comfortable margin with respect to the limit on the line average density of $10^{14} \kappa_a J \sim 10^{14} I/(\pi a^2)$, recently deduced by Greenwald.[20]

The plasma composition was determined as follows: The hydrogen isotopes in the initial gas, recycling, and gas puffing were 90% deuterium and 10% tritium. A spherical deuterium pellet of radius 1.1 mm was injected during ohmic heating to raise the density to 10^{20} m^{-3}. The pellet speed was set to make the pellet penetrate almost to the magnetic axis. Spherical tritium pellets of radius 2.1 mm were then injected during auxiliary heating to achieve the final operating density.

We chose to use a deuterium–dominated gas fill and recycling because this mode is likely to be characteristic of the initial tritium operation in CIT, in order to keep tritium inventory low. This type of low–tritium shot will probably be a critical operation phase of the machine, since full 50% tritium fill and recycling shots will be much less frequently allowed. A useful byproduct of this mode of operation is that depletion of tritium by recycling provides a natural burn control mechanism in our simulations.

The boundary conditions on the particle densities were fixed at 1/3 of the *initial* central values, with initially parabolic profiles. The boundary

temperatures were fixed at $T_{eo} = T_{io} = 0.1$ keV. The shape of the plasma boundary was given by the parametric representation $R = R_o \cos(a - \delta_a \cos\theta)$ and $Y = a\kappa_a \sin\theta$, where R is the major radius, Y is the height *off the midplane*, $0 \leq \theta < 2\pi$, and the coefficients are given in Table 1. During shutdown, the plasma was shifted outward by 4 cm, and pumping on the outer protective tiles was assumed to reduce the electron density as indicated in Fig. 1. For the empirical model we used a fixed $\langle Z_{eff} \rangle = 1.5$, with hydrogen isotope dilution computed assuming a carbon impurity.

Sawtooth reconnections in these simulations conserve helical flux and flatten density and temperature profiles.[15] The magnetic field energy destroyed during the reconnection heats the electrons in the mixing region. For numerical simplicity, we used a constant sawtooth period of 0.3 seconds in the reference simulations shown below. This is the value inferred at a temperature of 10 keV and an energy confinement time of 0.3 seconds from the scaling reviewed in Eq. (11.1.7) of Bateman.[21]

3. Results from Empirical Model

The curves in Fig. 2 show the evolution of plasma beta as a function of time for various values of the energy confinement parameter, α_{LH}, used in the empirical transport model [see Eq. (10)]. Here, beta is the ratio of the total plasma pressure (including the pressure from fast alpha particles) to the vacuum magnetic pressure

$$\langle \beta \rangle = \left\langle \frac{\sum_{species} nT}{B_o^2/2\mu_o} \right\rangle .$$

The range of simulations shown in Fig. 2 probably represents the minimum uncertainty for extrapolations using the present version of this model. (The much smaller uncertainties originally quoted for the coefficients in the formula[16] for τ_E^{aux} used in constructing this model may have resulted from an inappropriate statistical weighting procedure, as explained below.)

B. Semiempirical Model

1. Transport Coefficients

Semiempirical transport coefficients of the form

$$\chi_e = \frac{\alpha_t \rho}{R^2 \kappa^4 n_e^{7/8}} \left[\frac{(p_{th}/n_e^{0.95})}{(B\rho^{1/2}/q)^{0.8} Z_{eff}^{0.4}} \right]^t \left| \frac{d \ln p_{th}}{d \ln \rho} \right|^{t/2}, \tag{15}$$

$$\chi_i = 0.5\chi_e + \chi_i^{CH}(Z_{eff}), \tag{16}$$

$$D_a = 0.2\chi_e, \tag{17}$$

had previously been obtained[15] by applying the model of Pfeiffer and Waltz[17] to the local transport analysis of circular and noncircular plasmas. The particular choice for the fractional powers of n_e used in this model resulted from choosing the best global scaling of Pfeiffer and Waltz for low-density, circular, ohmic plasmas[17] and applying the quasineutrality dimensional constraint of Connor and Taylor[22] for a collisional, high-β plasma. The factor involving $d \ln p_{th}/d \ln \rho$ was inserted to produce correct radial profiles for models with $t > 0$.

The factor in the square brackets here scales globally as about

$$\frac{Ta^{3/2}}{(RI^{4/5} Z_{eff}^{2/5})} \tag{18}$$

and is about constant for ohmically heated plasmas. Calibrating such a model against data from experiments with auxiliary heating is known as "removing the ohmic constraint." The exponent t, obtained from scans of power (or plasma current) with auxiliary heating, is called the "confinement degradation exponent." For an almost identical model to that used here,[15] such a procedure gave $\alpha_0 = 4.0 \times 10^{19}$ $\pm 37\%$, $\alpha_1 = 2.1 \times 10^{33}$ $\pm 33\%$, and $\alpha_2 = 1.1 \times 10^{47}$ $\pm 45\%$ for models using the exponent $t = 0$, $t = 1$, and $t = 2$, respectively. The error bounds quoted here for each choice of α are the standard deviations between the best fit to data points and parameter scans from five different tokamaks.[15] Although the $t = 1$ model gives the best fit to this experimental data base, models with $0 \leq t \leq 2$ cannot be excluded on the basis of this analysis.

The scaling with elongation, κ, was determined separately by comparing values of $\langle\beta\rangle$ obtained from simulations against experimental data from the D-III tokamak[18,23] for a scan of auxiliary heated discharges with fixed safety factor at the boundary q_a and different elongations κ. The strong scaling with κ reflects the fact that both the total plasma current and average minor radius increase with κ for fixed values of half-width and q_a. An uncertainty of about ± 1 in the κ-scaling exponent calibrated at $\kappa \sim 1.5$ suggests a contribution to the uncertainty in the diffusion coefficients of about $\pm 33\%$ for CIT.

The semiempirical model is also designed to reproduce trends in impurity transport observed experimentally.[18] To implement the explicit transport of impurities in CIT simulations, the initial helium concentration of $n_{He}/n_e = 1\%$ was increased to a volume average of 8% after the first (deuterium) pellet, with a net influx of the shape indicated in Fig. 1. Since subsequent pellet injections dilute this initial helium concentration and since the fusion production of helium is small, this amount of helium should have relatively little effect on the fusion burn. Carbon was added to give an initial volume average effective charge of $\langle Z_{eff}\rangle = 1.5$. After the carbon concentration was diluted by hydrogen pellet injection, an additional carbon influx was used during auxiliary and alpha heating, as indicated in Fig. 1, to increase $\langle Z_{eff}\rangle$ back up to 1.4 by the end of the burn.

For numerical convenience, we added small terms to the diffusion coefficients which were particularly useful when explicitly transporting impurities. To correct for omission of small finite Larmor radius effects in the semiempirical diffusion coefficients and neoclassical fluxes, we added $2(\rho_{pi}/\rho)\chi_e$ to all of the diffusivities, where χ_e is the semiempirical diffusivity given above. Here $2\rho_{pi} = 2q(R/\rho)v_{thi}/\Omega_i$ is the poloidal gyrodiameter in a circular plasma, with thermal velocity $v_{thi} = (2T_i/\overline{m}_i)^{1/2}$ based on the local ion temperature (in Joules) and average ion mass, $\overline{m}_i$. The banana-plateau model used here is inappropriate for carbon near the plasma edge and causes numerical problems there. To the carbon anomalous diffusion coefficient only, we therefore add a term $(4\epsilon)^6\chi_e$, where χ_e is the semiempirical diffusivity given above.

2. Results using the Semiempirical Model

Here we document the effects of changing various modelling and machine parameters for CIT simulations using the semiempirical model just described. For the results shown here, the maximum volume average electron density was 8×10^{20} m^{-3}, which was the optimum indicated by preliminary global energy confinement studies. The time–dependent boundary conditions and constraints on the simulations are shown in Fig. 1.

Figures 3 through 5 show the time evolution of the profiles for the reference simulation using the semiempirical model. Figure 3 shows the electron temperature in keV along the vertical axis plotted against the flux surface half-width in meters along the horizontal axis and time in seconds along the receding axis. The duration of the 20 MW of auxiliary heating is indicated along the time axis. The electron temperature shows two distinct peaks in temperature. The first peak occurs during the low density phase, after the first small deuterium pellet, while the current is being ramped up. This relatively low-density high-temperature phase is used to freeze in the current profile to keep the sawtooth mixing radius small. The second temperature peak shows the effect of ignition which occurs after the tritium pellets have been injected and the volume-averaged electron density raised to 8×10^{20}m^{-3}. This peak persists for a second or so after the auxiliary heating is turned off. The temperature then decays as ignition is lost due to the combined effects of the loss of tritium (as it is replaced by deuterium), accumulation of carbon impurity (which enhances radiation loss and dilutes the hydrogenic densities), and the expanding sawtooth mixing radius (as more current penetrates to the center of the plasma).

Figure 4 shows the electron density profile as a function of flux-surface half-width and time. Pellet injection times are indicated along the time axis. It can be seen that the second and third pellets do not penetrate all the way to the magnetic axis, although diffusion, Ware pinch, and sawtooth oscillations rapidly fill in the central density profile. Between 10 and 12 seconds, the central density is sawtoothing between about 0.9 and 1.4×10^{21} electrons per cubic meter. Individual sawtooth oscillations are not well resolved on these profile versus time plots. After 9.5 seconds, the density is decreased during the shut-down operation.

Figure 5 shows the flux-surface-averaged current density profile as a function of flux-surface half-width and time. The duration of the current

ramp is indicated along the time axis. The gradually changing radial extent of the sawtooth mixing region shows up particularly well in this plot as a relatively flat central region out to an off-axis maximum. The negative current spike that marks the outer edge of the sawtooth mixing region can be seen in some of the time slices. The sharp central peak is the result of trapped particle effects in the neoclassical factor contributing to electrical resistivity. The rest of the current density profile evolves slowly on the sawtooth time scale, as current slowly diffuses into the plasma core. The edge of the current profile suddenly disappears as the total plasma current is reduced during the shut-down phase.

Among the uncertainties in this semiempirical model that we investigated in these simulations, it was found that the uncertainty in the confinement degradation exponent, t had the largest effect on ignition. The results for various values of t are shown in Fig. 6, where beta is plotted as a function of time during the discharge. In order to maintain approximately constant deposition profiles from the injected pellets for different values of the exponent t, the tritium pellet velocities were adjusted to be about $2t^{-1/2}$ km/s. The values of the coefficients $\alpha_{1/2}$ and $\alpha_{3/2}$ were interpolated from the values $\alpha_0 = 4.0 \times 10^{19}$, $\alpha_1 = 2.1 \times 10^{33}$, and $\alpha_{\cdot} = 1.1 \times 10^{47}$, which provided the best fit to experimental data.

For the model that provides the best fit to the available experimental data, (the model with exponent $t = 1$), the plasma β continues to rise after cessation of auxiliary heating at 9.3 s, indicating ignition, until the exchange of tritium for deuterium at the boundary reduces the fusion power production, providing a natural burn control mechanism. Ignition was stronger in identical simulations with balanced deuterium–tritium concentrations throughout the run. For more pessimistic choices of the confinement degradation exponent (for larger values of the exponent t), the fusion heating is still substantial, but it it is not sufficient to raising the plasma pressure (to ignite the plasma) after cessation of auxiliary heating.

The sensitivity of the simulations to various other parameters is indicated in Table 2. There we show the logarithmic derivative of the maximum achieved pressure, $\partial \ln\langle\beta\rangle / \partial \ln X$, for various parameters, X, around the reference point $t = 1$, $Z_{eff} = 1.5$, pellet speed = 2 km/s, heating location $\rho_{heat}/a = 0.5$, and sawtooth period 0.3 s. Variation of parameters like the impurity concentration, pellet velocity, and heating location, can evidently

all have a significant impact on ignition. (Since the plasma density source for a given size pellet is inversely proportional to its speed in the model used here,[24] varying the speed is equivalent to testing for sensitivity to uncertainties in the ablation rate.) By contrast, the start-up method chosen here has successfully kept the sawtooth inversion radius rather small, so varying the sawtooth period has relatively little impact in these simulations.[25]

III. GLOBAL ENERGY CONFINEMENT

Since there is a large body of data on global energy confinement, it is useful to compare the above results to extrapolations using global energy confinement scalings.

A. Pfeiffer-Waltz Type of Scaling

To our knowledge, there is only one such scaling which has been systematically calibrated against data from a variety of heating methods.[36] Our present application of this model assumes effectively equivalent heating profiles for ohmic, cyclotron resonance, and alpha heating, to give

$$\tau_E = \alpha_E n^{7/8} a^2 R_o^{9/4} \kappa_a \frac{R_o^{9/10} I^{4/5} Z_{eff}^{2/5}}{T_{keV} a^{6/5} \kappa_a^{2/5}} (1 + 0.7 q_{cyl}) \left(1 - \frac{1}{q_{cyl}^3}\right) \left(\frac{1}{1 + \frac{n^2}{n_{Mu}^2}}\right), \tag{19}$$

where $\alpha_E = 2.6 \times 10^{-20}$ in SI units, n is the volume average electron density, and T_{keV} is the density-weighted volume average of the average of the ion and electron temperatures in keV, the soft density limit for pellet fuelling is $n_{Mu} = 2.1 \times 10^{20} B/(q_{cyl} R_o)$,[26] and the cylindrical q-value q_{cyl} is defined just after Eq. (10). The terms in this equation represent a global energy confinement version of the Pfeiffer-Waltz scaling with the ohmic constraint removed,[17] followed by the heating efficiency factor $(1 + 0.7 q_{cyl})$, the sawtooth correction factor $(1 - 1/q_{cyl}^3)$, and a density limit correction $1/(1 + n^2/n_{Mu}^2)$. Unlike the semiempirical transport model, this confinement scaling had been systematically calibrated up to the density limit before the start of the present study. It is therefore interesting to survey the predictions of this scaling up to the very high densities potentially allowed by the new density limit formula derived by Greenwald et al.[20] These

results, shown in Fig. 7, were obtained by solving the stationary global energy balance (a 0-D calculation)

$$P_{aux} = \frac{3nTV}{\tau_E} + P_{brem} - P_{OH} - P_{\alpha}. \qquad (20)$$

Here P_{aux} is the auxiliary heating power plotted in Fig. 7, V is the plasma volume in an elliptical approximation, P_{brem} is the bremsstrahlung for a uniform plasma with $Z_{eff} = 1.5$, and the ohmic heating is obtained by applying Braginskii's formulas to a uniform plasma of electron density n, temperature T, and charge 1.5. (The details of these calculations are documented in a report by Singer and Ku.[27]) The fusion heating was obtained by integrating the cross sections of Hively et al.[28] over parabolic density and temperature profiles for concentric ellipses with constant ellipticity. In doing this, we assumed 60% deuterium in the hydrogen isotopes and a reactant fraction in the ions of 0.896 (appropriate to $n_{He}/n_e = 0.01$ and carbon to $Z_{eff} = 1.5$).

The power requirement at the saddle point in Fig. 7 is qualitatively compatible with the results in Fig. 2, where ignition is apparently just achieved in the analogous plasma transport model with 20 MW of auxiliary heating. Since these models were derived independently from two completely different types of data base, this agreement by better than a factor of two is encouraging. Figure 8 shows a quantitative comparison between the evolution of the global energy confinement time from a simulation using the reference $t = 1$ semiempirical model compared to the energy confinement time given by Eq. (19). The lower horizontal line in this figure shows the confinement time obtained from the global energy balance corresponding to the point $\times$ on Fig. 7 ($T = 9.3$ keV, $n = 8 \times 10^{20}\mathrm{m}^{-3}$ which are the parameters at maximum β in the reference transport simulation). A better comparison would use the new density limit by Greenwald[20] in place of n_{Mu} in Eq. (19) for τ_E. For parabolic density profiles, this gives a volume-averaged density limit of $0.75 \times 10^{20} I/(\pi a^2)$. The upper horizontal line shows τ_E from a global energy balance at $T = 9.3$ keV and $n = 8 \times 10^{20}\mathrm{m}^{-3}$ using this substitution for n_{Mu} in Eq. (19). The difference between these two formulations is relatively small at elongations $\kappa_a \lesssim 1.5$ where the two models have been calibrated, but becomes substantial at the higher elongation $\kappa_a = 2$ in the CIT design. At this level of comparison, the agreement

between the two methods of prediction seems as good as can be expected from the present accuracy of calibration for each model.

B. Other Global Energy Confinement Scalings

Of the many proposed global energy confinement scalings,[27,29] the one given above in Sect. II.A.1 has been used most extensively for studies of CIT performance.[19] It is important to note that extrapolation from the performance of operating tokamak experiments to CIT depends very sensitively on the exponents used in these scalings.

While the formula for τ_E^{aux} used in this model [Eq. (8)] was derived systematically from a data base, there is a potentially significant problem with the way the data was weighted in this derivation. In particular, the scaling as originally reported,

$$\tau_E^{aux} = 10^{-10.42\pm0.10} \frac{\kappa_a^{0.28\pm0.16} I^{1.24\pm0.06} (\overline{n}_e)^{0.26\pm0.03} a^{1.16\pm0.27} (R_o/a)^{1.65\pm0.42}}{B_o^{0.09\pm0.07} P^{0.58\pm0.03}} \tag{21}$$

was derived by weighting subsamples sorted by tokamak as if they were uncorrelated random samples from a normal distribution. In particular, the formula used for defining best fit parameters was

$$X = \frac{\sigma^2}{\sigma_i^2} X_i, \tag{22}$$

where X_i are the scaling exponents computed by regression analysis for a particular tokamak, and σ_i^2 are the associated variances. It is intuitively clear that the data from each tokamak are instead highly correlated. The variance between tokamaks can be shown, post facto, to be much larger for some of the scaling exponents from this data analysis than the variance for data from particular tokamaks.[30] Thus, repeated measurements of a single tokamak do not continue to reduce the overall variance as assumed in this weighting formula.

While still not statistically rigorous, a somewhat more appropriate method is to use an unweighted mean to combine the regressions reported by Kaye and Goldston[16] for each tokamak. (This assumes that the variance in data

from one tokamak is negligible compared to the variance between tokamaks.) This gives

$$\tau_E^{aux} = 10^{-10.42} \frac{\kappa_a^{0.23\pm0.33} I^{1.17\pm0.12} (\overline{n}_e)^{0.14\pm0.14} a^{1.16\pm0.27} (R_o/a)^{1.65\pm0.42}}{B_o^{0.02\pm0.12} P^{0.55\pm0.11}}. \quad (23)$$

The error estimates in this formula are the quantitative basis for the statement above that there are sizeable errors involved in extrapolating the empirical transport model to CIT. For example, a power-scaling exponent of $\alpha_P = 0.55 \pm 0.11 = (0.44, 0.55, 0.66)$ can be seen from global power balance to be roughly comparable to a confinement degradation exponent in the semiempirical model of $t \sim \alpha_P/(1-\alpha_P) \sim (0.8, 1.2, 1.9)$. This may seem obvious, but the implications for making systematic progress in reducing the uncertainties in such extrapolations are significant.

There is an ongoing effort to determine more accurate global energy confinement scalings from the increasing wealth of experimental data. Since Ohmic heating is important in the early stages of CIT discharges, it is particularly important to determine the transition between the Ohmic heating and the auxiliary heating energy confinement times. The transition given by Eq. (10) may be too gradual. Finally, we have yet to learn whether or not the heating from fusion alpha particles degrades energy confinement as much as other forms of auxiliary heating.

IV. DISCUSSION

The most important result reported here is that ignition is obtained for the CIT parameters using a transport model previously calibrated against L-mode experimental data. The semiempirical $t = 1$ model used here is perhaps the best available predictive model fit to experimental data, since it has been systematically derived from a reasonably broad and detailed data base. Moreover, the simulations presented here were done with a realistic start-up scenario and reasonably conservative assumptions about tritium inventory in the limiters, heating profiles, pellet velocity, and impurity contamination. We would suggest that this model gives the most accurate assessment of the likely plasma performance, assuming the present design parameters for the toroidal field, plasma current, and heating power.

These encouraging conclusions are presently tempered by a large degree of uncertainty concerning the stability of the plasma profiles, the accuracy of the source calculations, and the validity of the transport model. Potential instabilities include double tearing modes, density limit disruptions, fishbones, pressure-driven external kinks, and ballooning modes. Since monotonic $q(\rho)$ profiles are maintained during start-up in the simulations presented here, there is no particular reason to suspect that these profiles would be subject to double tearing instabilities. This is important, since redistribution of the poloidal flux could increase the sawtooth mixing radius, broadening the profiles, and consequently making it more difficult to reach ignition. Due to the current ramp-up scenario used in these simulations, the sawtooth mixing radius starts out small and gradually grows to about half the plasma half-width (or one quarter of the plasma volume) while the plasma is igniting. All other things being equal, the smaller the sawtooth mixing radius and the more peaked the temperature and density profiles, the easier it is to reach ignition.

Conditions conducive to density limit disruptions occur only near the end of shutdown, because we do not pump out carbon as we ramp the density down. As the plasma ramps down, carbon near the plasma edge recombines to C^{+2} and increases the radiated power. This is a well-documented signature of the approach to density limit disruptions in at least one tokamak.[31] This condition occurs only near the end of shutdown in our simulations, when the magnetic and kinetic energy are about two orders of magnitude below their maxima. Since we keep the density well below the limit recently deduced by Greenwald et al.,[20] density limits should not be a significant factor in determining the validity of our simulations.

Fishbone instabilities are rapid oscillations which can be driven by nonthermal ion distributions. When the maximum $\langle\beta\rangle$ is achieved in the reference simulation with the $t = 1$ semiempirical model, the contribution due to fast alphas is $\langle\beta_\alpha\rangle = 0.3\%$ absolute. To test theories of the interaction of fusion products with thermal plasma is one of the main purposes of the CIT, so the possibility of such instabilities is not *per se* undesirable. It would, nevertheless, be desirable to have a detailed analysis of such instabilities for the types of profiles generated here. The BALDUR code produces diagnostics which would be useful in such a study, but this is beyond the scope of the present paper.

Pressure-driven external kink modes have been associated with disruptions in tokamaks at high $\langle\beta\rangle$. Work is under way to analyze the stability of our simulated profiles to these modes. The presence of a close-fitting, low-resistivity vacuum vessel, which is planned for CIT, should have a significant stabilizing effect on such instabilities.

The profiles produced from the reference $t = 1$ semiempirical simulations described above have been found to be unstable to ideal MHD ballooning modes within the central low shear sawtooth mixing region. A more relevant analysis should result from including kinetic effects such as finite Larmor radii and trapped particles. A code exists which includes such effects in a fairly complete manner and also produces estimates of the resulting quasilinear particle and energy fluxes.[32] Since the semiempirical model reflects an attempt to experimentally calibrate fluxes dependent on the pressure profile steepness, an analysis with such a code might be particularly instructive.

Uncertainties in the source terms used for these simulations will be partly resolved by continuing improvements in models of cyclotron resonance heating, pellet ablation, and neutral gas transport. The most difficult task will be to predict impurity sources and transport. Here we only note that values of $\langle Z_{eff}\rangle$ similar to those used for these simulations have routinely been achieved at high plasma densities. A thorough empirical study aimed at extrapolating present results on this topic to CIT would be useful.

The validity of the transport models depends on how well they are calibrated and how appropriately they are applied. Fortunately, high-power heating in the JET experiment should very nearly reproduce all of the dimensionless thermal plasma parameters (β, ν_{e*}, ρ_{pi}/ρ, ϵ, q, ...) required in CIT. An exception is the ratio of the Debye length to the machine dimensions, but this does not play a role in most theories of plasma transport in tokamaks. It should, therefore, be appropriate to apply models calibrated against this and other data to predictions for CIT if the models obey the quasineutrality constraint and have been tested against a wide variety of parameter scans.[33] The semiempirical models described above are explicitly designed to make such similarity transformations. The empirical model used here and several of the other transport models[34,35] currently in use are also nearly or exactly compatible with the quasineutrality dimensional

constraint. Of particular interest are two theory-based models which have been qualitatively[34] or quantitatively[18] compared to a variety of experimental data. At present, both of these models use an empirical constraint to determine the scaling with plasma current, a scaling which is crucial for CIT. This and the fact that these models are still being experimentally calibrated made them less attractive for the present simulations, but models of this type may rapidly become more useful for predictive modelling. For all the models, however, more statistically rigorous testing against a wider data base will be necessary before quantitative statements can be made about their accuracy.

While our studies indicate that the most likely outcome of limiter operation at full CIT parameters would be an increase in the plasma pressure after shutting off auxiliary heating (*i.e.*, ignition), there are, fortunately, two modes of CIT operation which allow for better performance, as a "hedge" against these uncertainties. First, better control of the tritium mix might be achieved by pumping deuterium during the discharge or by preconditioning the graphite liner tiles with tritium. Additional tritium pellets or more tritium in the recycled gas would then improve the deuterium-tritium mix, albeit at the expense of a larger tritium inventory. Detailed analysis of this problem will require a rather sophisticated coupling between models of the core plasma, neutral gas, and surface structures.

A second method of improving plasma performance is operation with a poloidal divertor. This may give better energy confinement and/or impurity control. Recent comparison of inner-wall limiters and divertors in an open configuration not too dissimilar from that planned for CIT show only a modest improvement in confinement with the divertor (on the order of 10%).[36] But differences between divertors and rail limiters on other machines have been more dramatic, and the reasons for these differences are not fully understood. To address this question for CIT, it would be desirable to have an appropriate experimentally calibrated model of divertor plasmas. Shear stabilization of transport at low collisionality is presently being added to the semiempirical model in the BALDUR code to study this problem.

Acknowledgment

This work was supported by the U.S. Department of Energy Contract No. DE–AC02–76–CHO–3073.

It is a pleasure to acknowledge valuable discussions with D. Post, W. Reiersen, D. Mikkelsen, and J. Mandrekus.

References

[1]J. Sheffield, M. Bell, K. H. Burrell, P. Colestock M. Greenwald, J. Hosea, W. A. Houlberg, S. Kaye, P. Liewer, N. Ohyabu, M. Petravic, D. Post, D. Ross, S. D. Scott, C. Singer, R. Stambough, N. A. Uckan, H. Weitzner, K. M. Young, Physics Guidelines for the Compact Ignition Experiment, Proc. ANS Conf. (Reno, June, 1986), in press.

[2]W. Reiersen, Princeton Plasma Physics Laboratory private communication "Proposed CIT Design Point (R = 1.324 m)," memorandum EAD-1516 (1986).

[3]W. A. Houlberg, Plasma Engineering Assessments of Compact Ignition Experiments, Proc. Eleventh Symp. on Fusion Engineering (IEEE, Austin, 1985) Vol. 1, p. 50.

[4]C. E. Singer, L. P. Ku, G. Bateman, F. Seidl, and M. Sugihara, Physics of Compact Ignition Designs, Proc. Eleventh Symp. on Fusion Engineering (IEEE, Austin, 1985) Vol. 1, p. 41.

[5]G. Bateman, "Algorithms for 1-1/2-D Transport," International Center for Theoretical Physics, Spring College on Plasma Physics (Trieste, Italy, 1985) in press.

[6]C. E. Singer D. E. Post, D. R. Mikkelsen, M. H. Redi, A. McKenney, A. Silverman, F. G. P. Seidl, P. H. Rutherford, R. J. Hawryluk, W. D. Langer, L. Foote, D. B. Heifetz, W. A. Houlberg, M. H. Hughes, R. V. Jensen, G. Lister, and J. Ogden. "BALDUR: A One-dimensional Plasma Transport Code," Princeton Plasma Physics Laboratory Report PPPL-2073 (1986), submitted to Computer Phys. Communications.

[7]S. P. Hirshman and J. C. Whitson, Phys. Fluids **26** (1983) 3553.

[8]S. P. Hirshman and H. K. Meier, Phys. Fluids **28** (1985) 1387.

[9]S. P. Hirshman and D. K. Lee, Comp. Phys. Comm. **39** (1986) 161–172.

[10]R. Hawryluk, S. Suckewer, and S. Hirshman, Nucl. Fusion **19** (1979) 607.

[11]C. S. Chang and F. L. Hinton, Phys. Fluids **25** (1982) 1493.

[12]D. F. Düchs, D. E. Post, and P. H. Rutherford, Nucl. Fusion **17** (1977) 3.

[13]P. H. Rutherford, Princeton Plasma Physics Laboratory private communication (1985).

[14]M. Hughes and D. Post, J. Comp. Phys. **28** (1978) 43.

[15]D. R. Mikkelsen, Princeton Plasma Physics Laboratory private communication (1985).

[16]S. M. Kaye and R. J. Goldston, Nucl. Fusion **25** (1985) 65.

[17]W. Pfeiffer and R. Waltz, Nucl. Fusion **19** (1979) 51.

[18]Ignitions Physics Study Group Report on Testing Predictive Transport Models, in preparation (1986).

[19]N. A. Uckan, J. Sheffield, and E. C. Selcow, "A Simple Contour Analysis of Ignition Conditions and Plasma Operating Regimes in Tokamaks," Proc. Eleventh Symp. on Fusion Engineering (IEEE, Austin, 1985) Vol. 1, p. 350.

[20]M. Greenwald et al., MIT Plasma Fusion Center Report FPC/JA-86-22 (1986).

[21]G. Bateman, *MHD Instabilities*, (MIT Press, Cambridge, 1978).

[22]J. W. Connor and J. B. Taylor, Nucl. Fusion **19** (1979) 51.

[23]S. Ejima, T.W. Petrie, A.C. Riviere, T.R. Angel, C.J. Armentrout *et al.*, Nucl. Fusion **22** (1982) 1627.

[24]W.A. Houlberg, M.A. Iskra, H.C. Howe, and S.E. Attenberger, Oak Ridge National Laboratory Report ORNL/TM-6549 (1979).

[25]G. Bateman, "Delaying Sawtooth Oscillations in the Compact Ignition Tokamak," Princeton Plasma Physics Laboratory Report PPPL-2373 (September 1986). Fusion Technology (in press).

[26]M. Sugihara and C. E. Singer, "Energy Confinement in Tokamaks," Nucl. Fusion **26** (1986) 1547.

[27]C. E. Singer and L. P. Ku, "Computing Energy Confinement Times," Princeton Plasma Physics Laboratory Report PPPL-TM-374 (1986).

[28]L. Hively, Nucl. Fusion **17** (1977) 873.

[29]S. Kaye, Phys. Fluids **28** (1985) 2327.

[30]C. E. Singer, presented at Ignition Physics Study Group Workshop (Austin, Jan. 1986).

[31]H. Niedermeyer, K. Behringer, K. Bernhardi, A. Eberhagen, G. Fussman *et al.*, "Prior to High Density Disruptions in ASDEX," Controlled Fusion and Plasma Physics (Proc. Eleventh European Conference, Aachen, 1983) Part I, p. 43.

[32]W. M. Tang, G. Rewoldt, and L. Chen, "Microinstabilities in Weak Density Gradient Tokamak Systems," Phys. Fluids **29** (1986) 3715.

[33]C. E. Singer, J. Fusion Energy **3** (1983) 231.

[34]R. E. R. Dominguez and R. E. Waltz, "Tokamak Transport Code Simulations with Drift Wave Models," GA Technologies Report GA-18184 (1986).

[35]W. Tang, "Microinstability-Based Model for Anomalous Thermal Confinement in Tokamaks," Princeton Plasma Physics Laboratory Report PPPL-2311 (1986).

[36]J.C. DeBoo, R.J. Groebner, Doublet III Physics, Operations, and Neutral Beam Groups, "Energy Confinement Experiments on Doublet III with High Power Neutral Beam Heating," Controlled Fusion and Plasma Physics (Proc. Twelth European Conference, Budapest, 1985) vol. 1, p. 2.

Table 1. CIT Parameters

Parameter	Symbol (Units)	Value
Major Radius	R_o (m)	1.32
Midplane Half-width	a (m)	0.43
Elongation	κ_a	2.0
Triangularity	δ_a	0.4
Max. Toroidal Field	B_o (T)	10.4
Max. Plasma Current	I (MA)	10.0
Helium fraction	n_{He}/n_e	0.08 (before T pellets) 0.01 (after T pellets)
Z_{eff} (Carbon and Helium)	Z_{eff}	1.4
Tritium pellet speed	(km/s)	2.0
Tritium pellet radius	(mm)	2.1–2.35
Number of tritium pellets		2

Table 2. Sensitivity of Ignition to Variation of Parameters

Parameter, X	$\partial \ln\langle\beta\rangle_{max}/\partial \ln X$
Confinement Exponent, t	-3.85
Heating location, ρ_{heat}/a	-1.97
$Z_{eff} - 1$	-1.44
Pellet speed	1.13
Sawtooth period	0.01

Figures

FIG. 1. Time evolution of the boundary conditions and constraints for reference CIT simulations. The solid lines show the density programming for simulations using the empirical model. The short–dashed lines show the density programming for simulations using the semiempirical model.

FIG. 2. Time evolution of $\langle\beta\rangle$ for various values of the energy parameter, α_{LH} in the empirical model. Note, $\alpha_{LH} = 1$ for the Kaye-Goldston L-mode scaling (KG-L), $\alpha_{LH} = 2$ for the normal H-mode scaling (KG-H), and $\alpha_{LH} = 4$ for superior H-mode scaling (KG-2H).

FIG. 3. Time evolution of the electron temperature profile for the reference simulation using the semiempirical model. The time duration of auxiliary heating is indicated.

FIG. 4. Time evolution of the electron density profile for the reference semiempirical simulation. Pellet injection times are indicated.

FIG. 5. Time evolution of the flux-surface-averaged current density profile for the reference semiempirical simulation. Duration of the current ramp is indicated.

FIG. 6. Time evolution of $\langle\beta\rangle$ for various values of the confinement degradation exponent parameter, t, in the semiempirical model.

FIG. 7. Auxiliary heating power (in MW) required to maintain CIT plasmas in thermal equilibrium using a global version of Pfeiffer–Waltz scaling with the ohmic constraint removed. Here $\times$ marks the conditions under which the maximum $\langle\beta\rangle$ was achieved in the reference transport simulation of Fig. 2 using the $t = 1$ semiempirical model. The hyperbola marked $\beta = 0.035I/(aB)$ shows an upper stability limit which fits a variety of experiments without close–fitting conducting shells.

FIG. 8. Comparison of global energy confinement times from transport modelling and global energy balances.

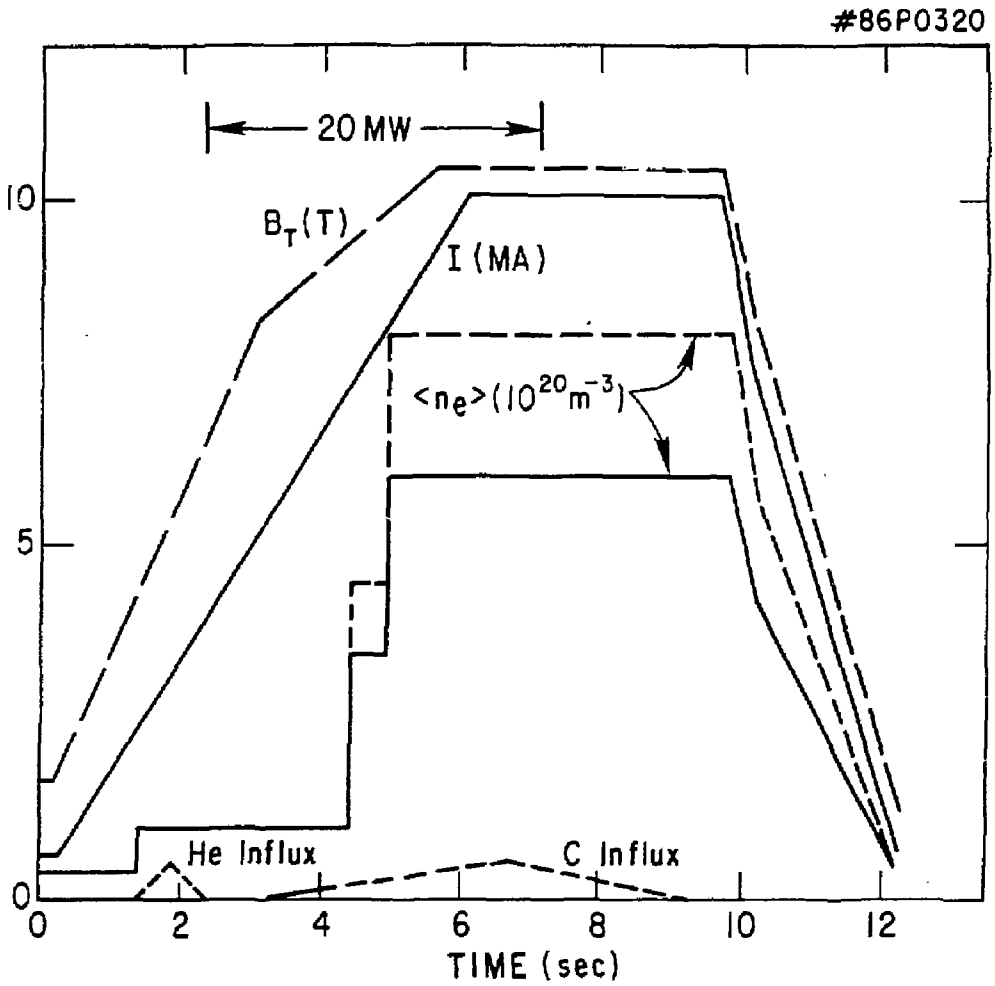

FIG. 1. Time evolution of the boundary conditions and constraints for reference CIT simulations. The solid lines show the density programming for simulations using the empirical model. The short-dashed lines show the density programming for simulations using the semiempirical model.

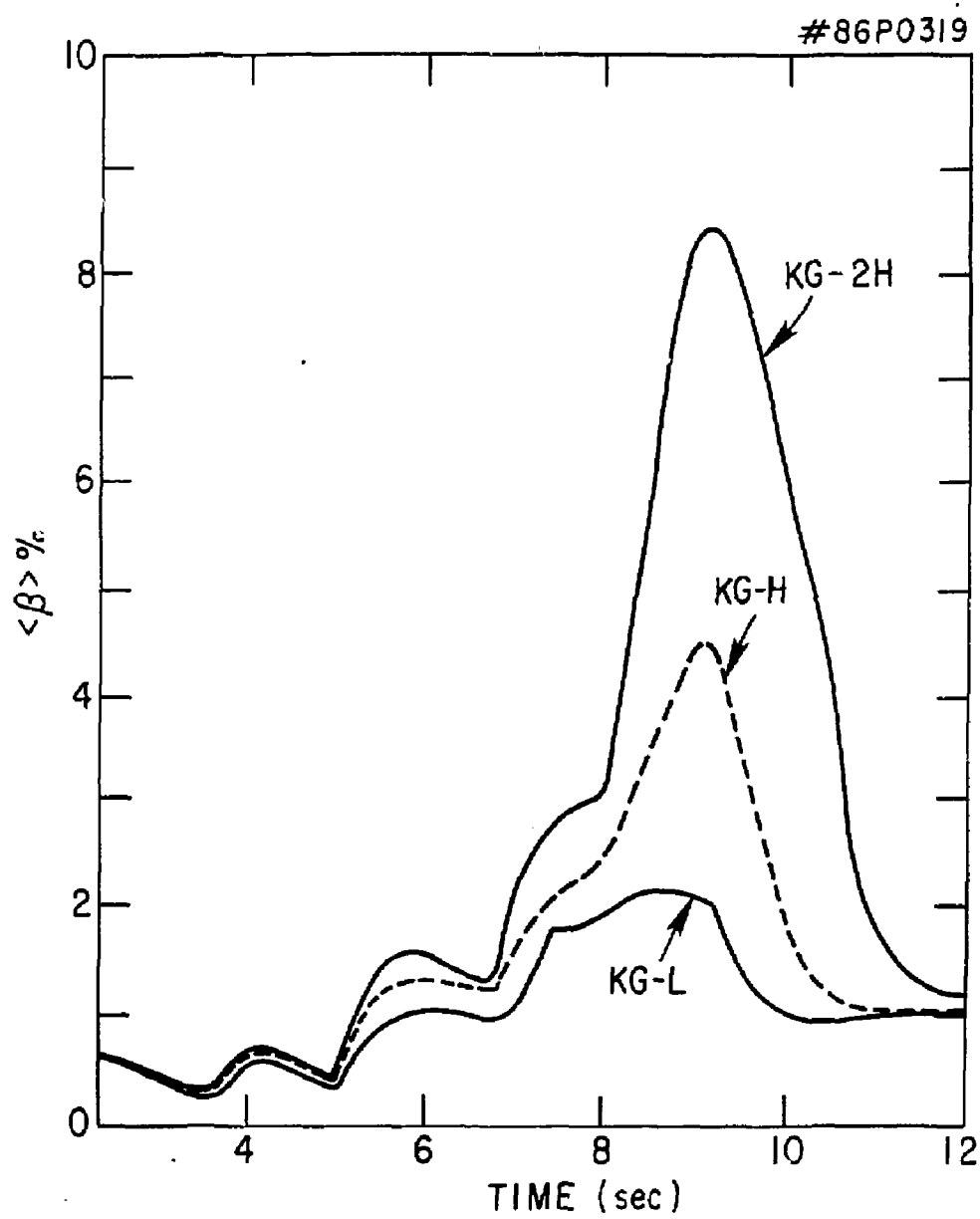

FIG. 2. Time evolution of $\langle\beta\rangle$ for various values of the energy parameter, α_{LH} in the empirical model. Note, $\alpha_{LH} = 1$ for the Kaye-Goldston L-mode scaling (KG-L), $\alpha_{LH} = 2$ for the normal H-mode scaling (KG-H), and $\alpha_{LH} = 4$ for superior H-mode scaling (KG-2H).

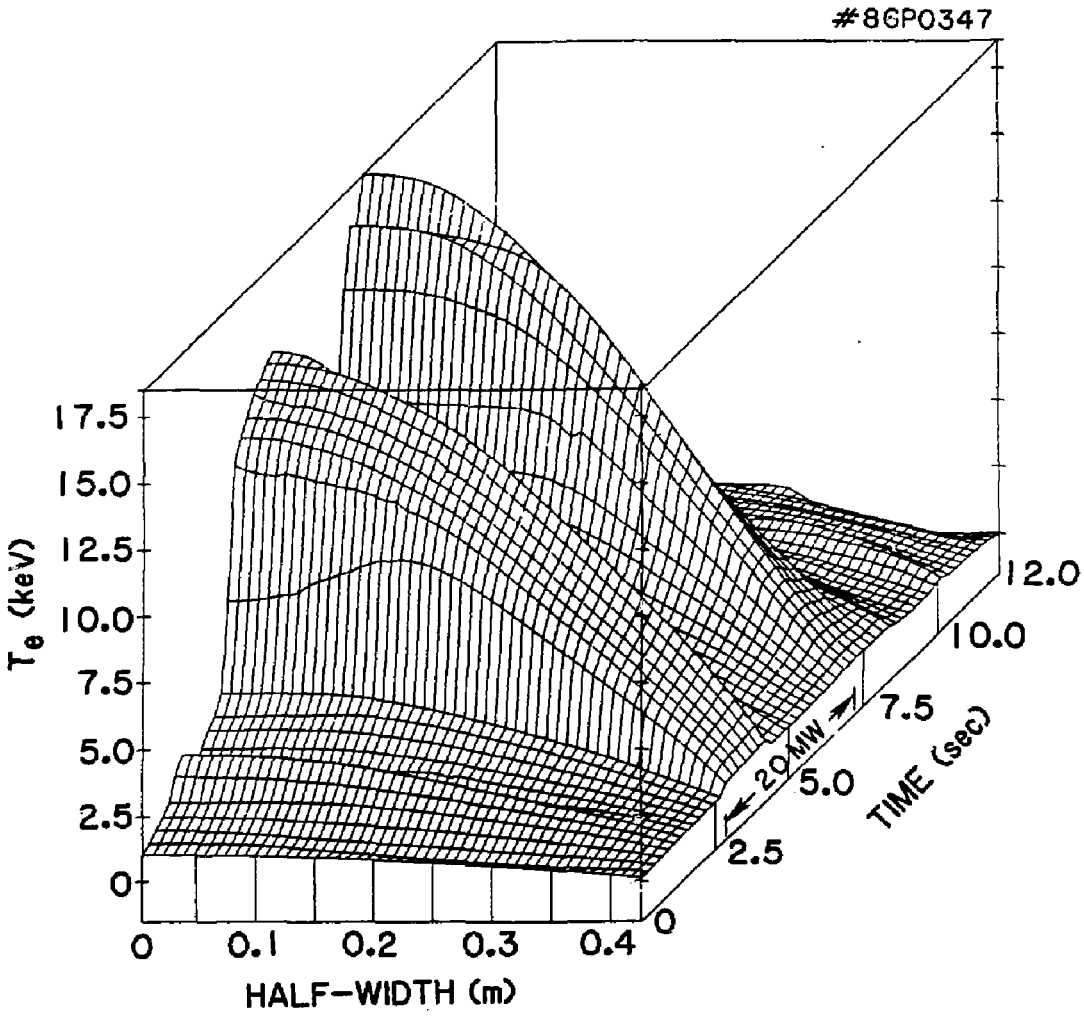

FIG. 3. Time evolution of the electron temperature profile for the reference simulation using the semiempirical model. The time duration of auxiliary heating is indicated.

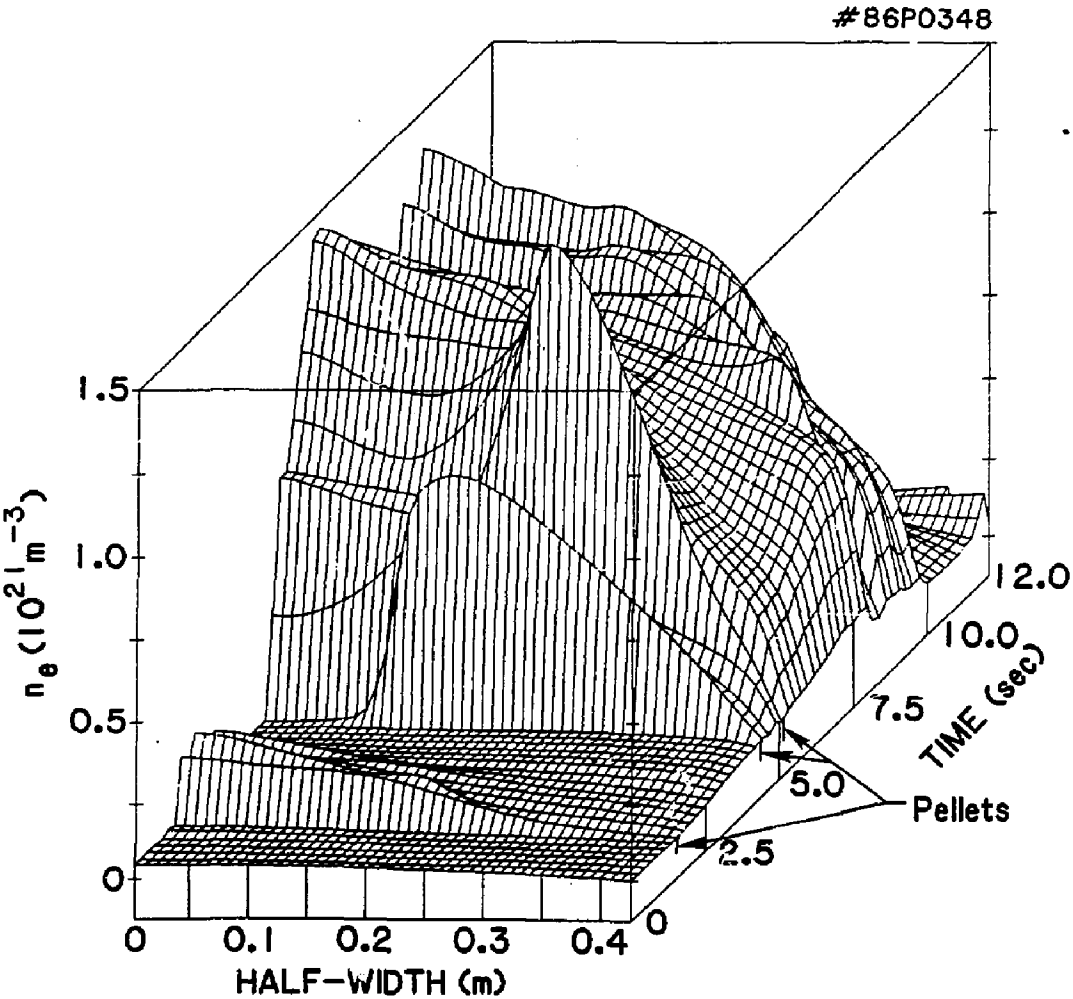

FIG. 4. Time evolution of the electron density profile for the reference semiempirical simulation. Pellet injection times are indicated.

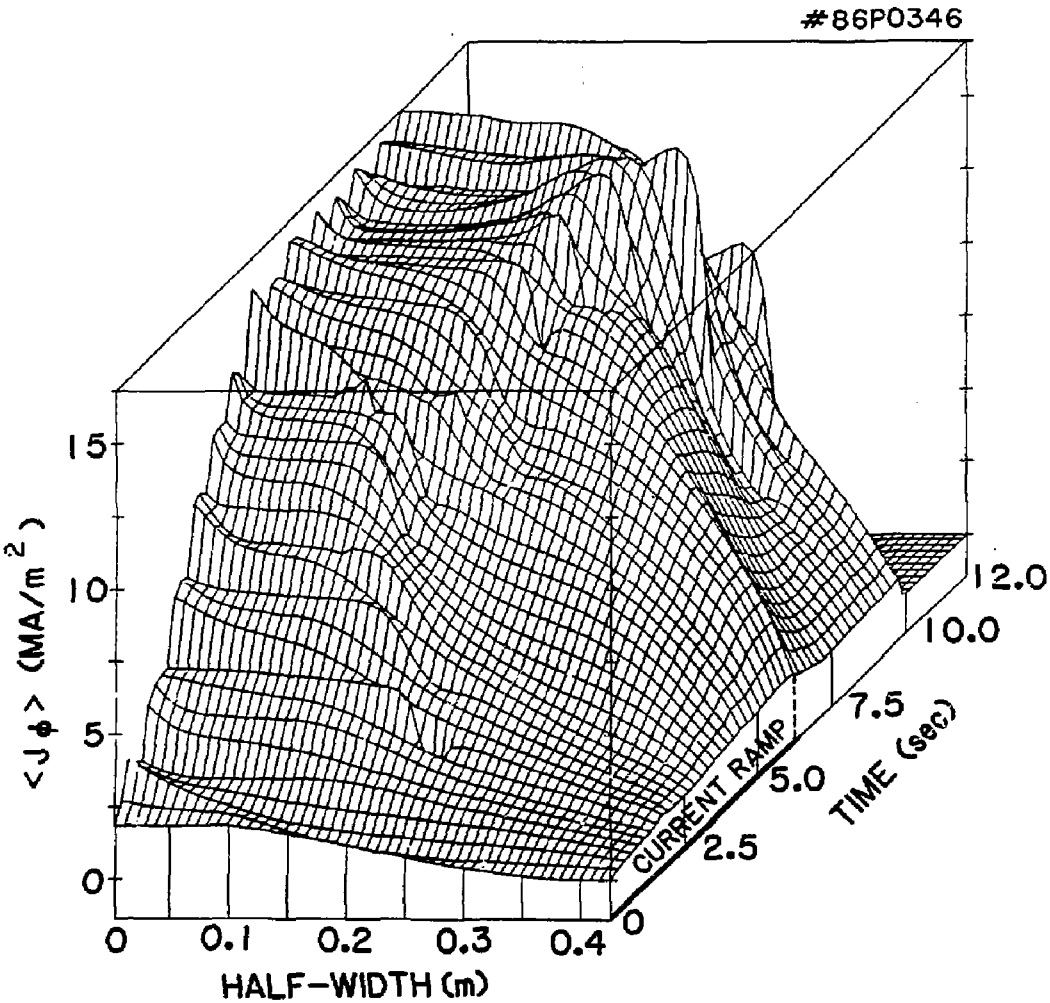

FIG. 5. Time evolution of the flux-surface-averaged current density profile for the reference semiempirical simulation. Duration of the current ramp is indicated.

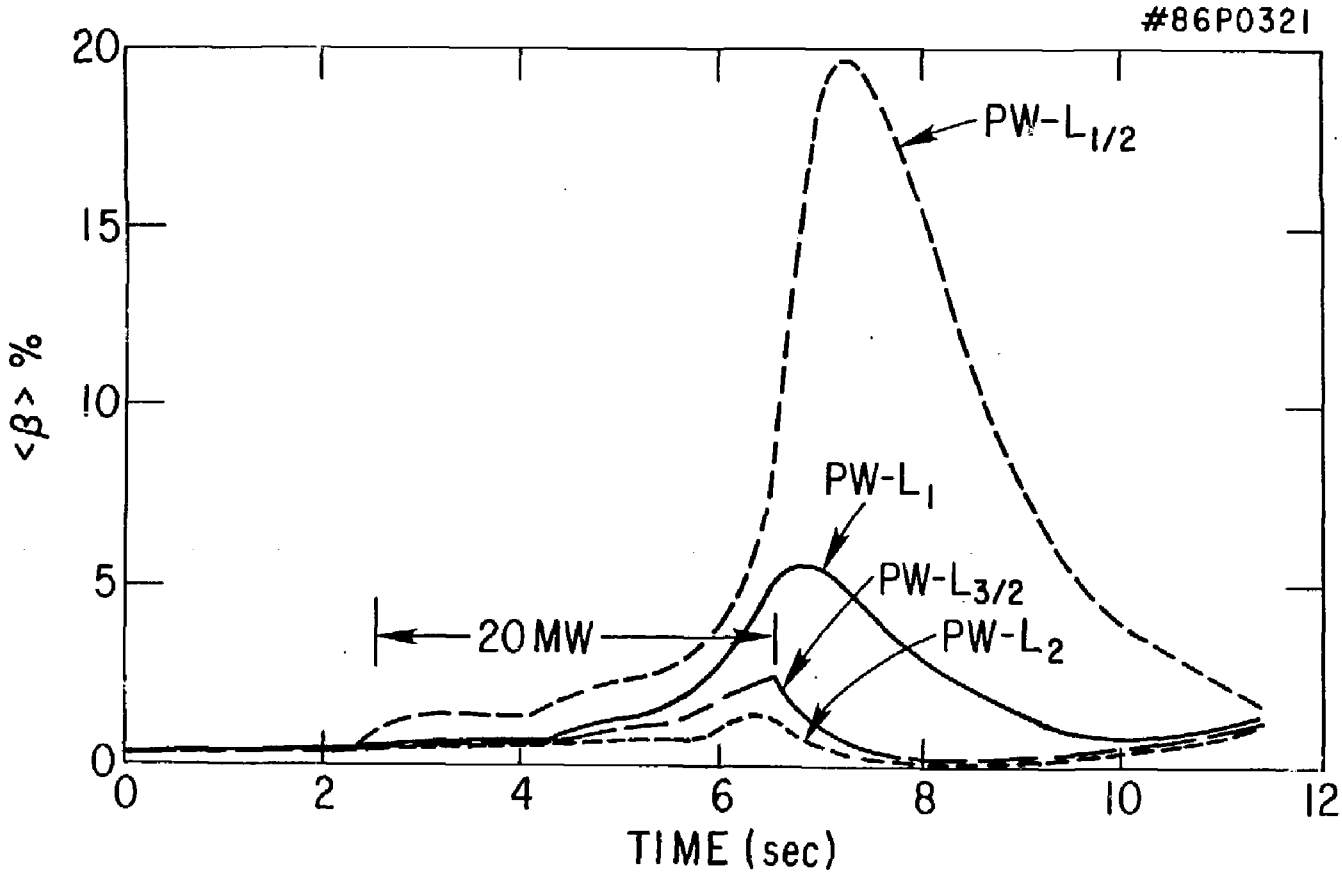

FIG. 6. Time evolution of $\langle\beta\rangle$ for various values of the confinement degradation exponent parameter, t, in the semiempirical model.

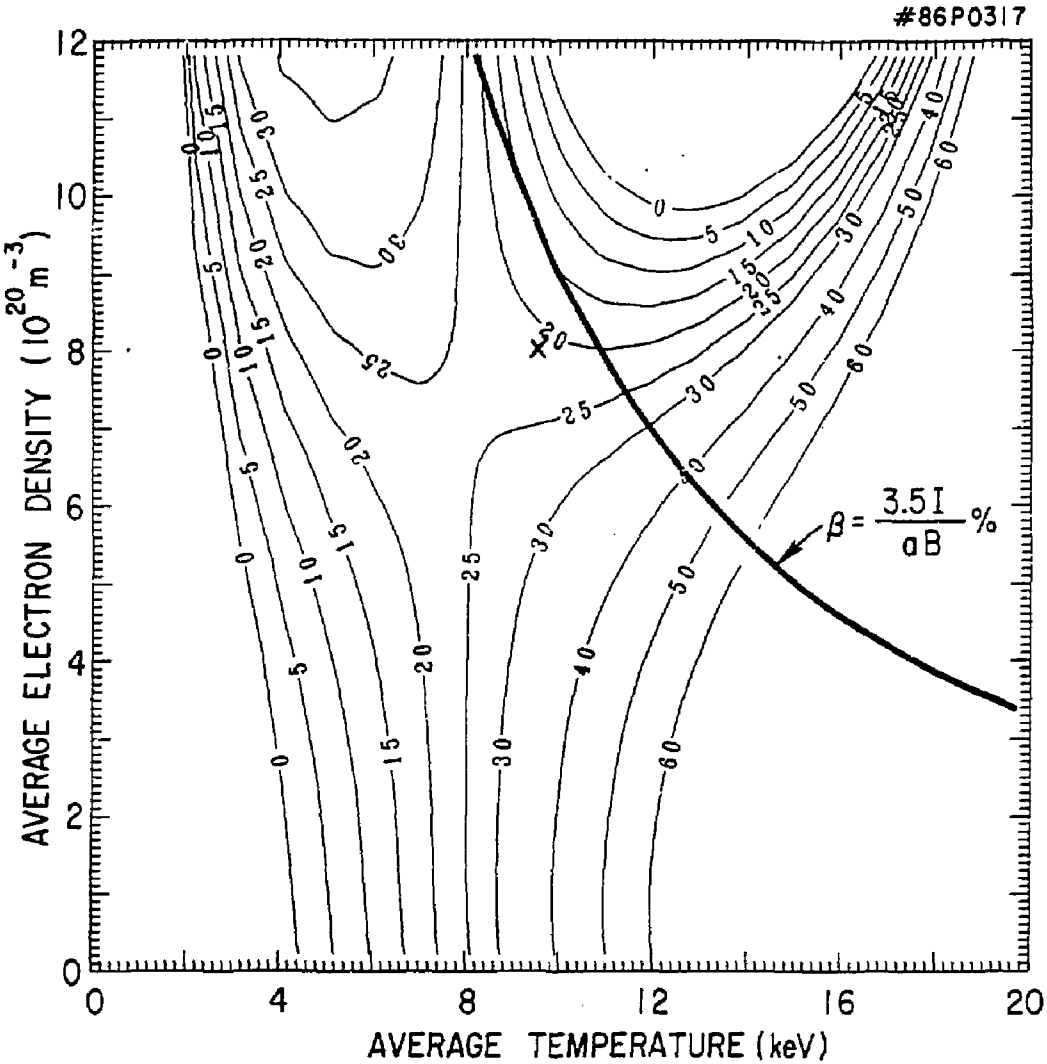

FIG. 7. Auxiliary heating power (in MW) required to maintain CIT plasmas in thermal equilibrium using a global version of Pfeiffer–Waltz scaling with the ohmic constraint removed. Here × marks the conditions under which the maximum (β) was achieved in the reference transport simulation of Fig. 2 using the $t = 1$ semiempirical model. The hyperbola marked $\beta = 0.035I/(aB)$ shows an upper stability limit which fits a variety of experiments without close–fitting conducting shells.

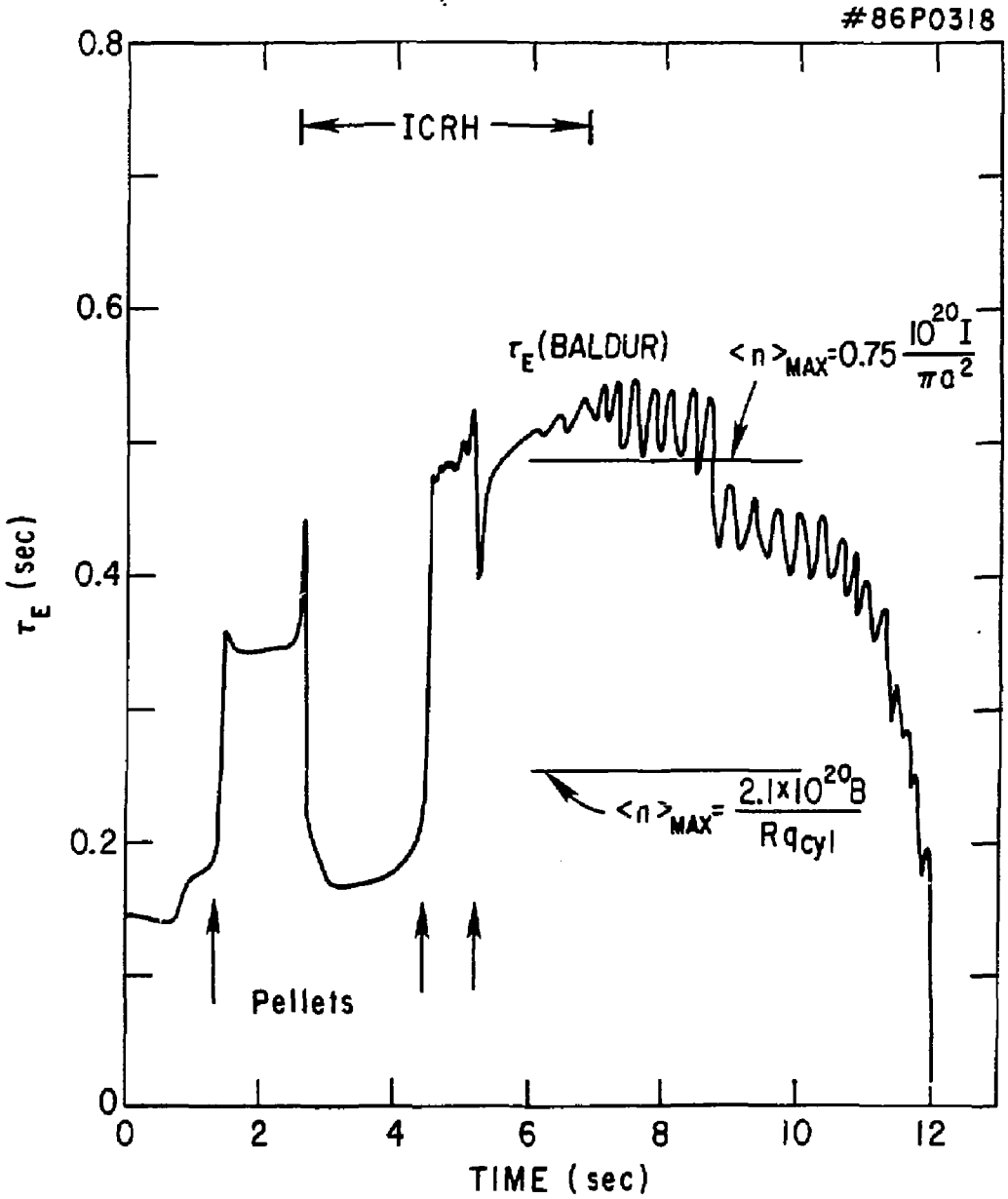

FIG. 8. Comparison of global energy confinement times from transport modelling and global energy balances.

EXTERNAL DISTRIBUTION IN ADDITION TO UC-20

Dr. Frank J. Paoloni, Univ of Wollongong, AUSTRALIA
Prof. M.H. Brennan, Univ Sydney, AUSTRALIA
Plasma Research Lab., Australian Nat. Univ., AUSTRALIA
Prof. I.R. Jones, Flinders Univ., AUSTRALIA
Prof. F. Cap, Inst Theo Phys, AUSTRIA
Prof. M. Heindler, Institut fur Theoretische Physik, AUSTRIA
M. Goossens, Astronomisch Instituut, BELGIUM
Ecole Royale Militaire, Lab de Phys Plasmas, BELGIUM
Com. of European, Dg XII Fusion Prog, BELGIUM
Prof. R. Boucique, Laboratorium voor Natuurkunde, BELGIUM
Dr. P.H. Sakanaka, Univ Estadual, BRAZIL
Instituto De Pesquisas Espaciais-INPE, BRAZIL
Library, Atomic Energy of Canada Limited, CANADA
Dr. M.P. Bachynski, MPB Technologies, Inc., CANADA
Dr. H.M. Skarsgard, Univ of Saskatchewan, CANADA
Dr. H. Barnard, University of British Columbia, CANADA
Prof. J. Teichmann, Univ. of Montreal, CANADA
Prof. S.R. Sreenivasan, University of Calgary, CANADA
Prof. Tudor W. Johnston, INRS-Energie, CANADA
Dr. C.R. James, Univ. of Alberta, CANADA
Dr. Peter Lukac, Komenskeho Univ, CZECHOSLOVAKIA
The Librarian, Culham Laboratory, ENGLAND
Mrs. S.A. Hutchinson, JET Library, ENGLAND
C. Mouttet, Lab. de Physique des Milieux Ionises, FRANCE
J. Radet, CEN/CADARACHE - Bat 506, FRANCE
Dr. Tom Mual, Academy Bibliographic, HONG KONG
Preprint Library, Cent Res Inst Phys, HUNGARY
Dr. B. Dasgupta, Saha Inst, INDIA
Dr. R.K. Chhajlani, Vikram Univ. INDIA
Dr. P. Kaw, Institute for Plasma Research, INDIA
Dr. Phillip Rosenau, Israel Inst Tech, ISRAEL
Prof. S. Cuperman, Tel Aviv University, ISRAEL
Librarian, Int'l Ctr Theo Phys, ITALY
Prof. G. Rostagni, Univ Di Padova, ITALY
Miss Clelia De Palo, Assoc EURATOM-ENEA, ITALY
Biblioteca, del CNR EURATOM, ITALY
Dr. H. Yamato, Toshiba Res & Dev, JAPAN
Prof. I. Kawakami, Atomic Energy Res. Institute, JAPAN
Prof. Kyoji Nishikawa, Univ of Hiroshima, JAPAN
Direc. Dept. Lg. Tokamak Res. JAERI, JAPAN
Prof. Satoshi Itoh, Kyushu University, JAPAN
Research Info Center, Nagoya University, JAPAN
Prof. S. Tanaka, Kyoto University, JAPAN
Library, Kyoto University, JAPAN
Prof. Nobuyuki Inoue, University of Tokyo, JAPAN
S. Mori, JAERI, JAPAN
M.H. Kim, Korea Advanced Energy Research Institute, KOREA
Prof. D.I. Choi, Adv. Inst Sci & Tech, KOREA
Prof. B.S. Liley, University of Waikato, NEW ZEALAND
Institute of Plasma Physics, PEOPLE'S REPUBLIC OF CHINA
Librarian, Institute of Phys., PEOPLE'S REPUBLIC OF CHINA
Library, Tsing Hua University, PEOPLE'S REPUBLIC OF CHINA
Z. Li, Southwest Inst. Physics, PEOPLE'S REPUBLIC OF CHINA
Prof. J.A.C. Cabral, Inst Superior Tecn, PORTUGAL
Dr. Octavian Petrus, AL I CUZA University, ROMANIA
Dr. Johan de Villiers, Plasma Physics, AEC, SO AFRICA
Prof. M.A. Hellberg, University of Natal, SO AFRICA
Fusion Div. Library, JEN, SPAIN
Dr. Lennart Stenflo, University of UMEA, SWEDEN
Library, Royal Inst Tech, SWEDEN
Prof. Hans Wilhelmson, Chalmers Univ Tech, SWEDEN
Centre Phys des Plasmas, Ecole Polytech Fed, SWITZERLAND
Bibliotheek, Fom-Inst Voor Plasma-Fysica, THE NETHERLANDS
Dr. O.D. Ryutov, Siberian Acad Sci, USSR
Dr. G.A. Eliseev, Kurchatov Institute, USSR
Dr. V.A. Glukhikh, Inst Electro-Physical, USSR
Dr. V.T. Tolok, Inst. Phys. Tech. USSR
Dr. L.M. Kovrizhnykh, Institute Gen. Physics, USSR
Prof. T.J.M. Boyd, Univ College N Wales, WALES
Nuclear Res. Establishment, Julich Ltd., W. GERMANY
Bibliothek, Inst. Fur Plasmaforschung, W. GERMANY
Dr. K. Schindler, Ruhr Universitat, W. GERMANY
ASDEX Reading Rm, IPP/Max-Planck-Institut fur Plasmaphysik, W. GERMANY
Librarian, Max-Planck Institut, W. GERMANY
Prof. R.K. Janev, Inst Phys, YUGOSLAVIA